Colloid Polym Sci (2016) 294:755–765
DOI 10.1007/s00396-016-3833-7

ORIGINAL CONTRIBUTION

# Comparative study on interaction of N-PBS and cellulose derivatives by dynamic simulation

**Xiao-Ling Xu[1] · Min Zhang[1] · Lei Wang[1] · Shan Duan[1] · Ji-Qing Song[2,3]**

Received: 27 August 2015 / Revised: 10 December 2015 / Accepted: 10 January 2016 / Published online: 21 January 2016


**Abstract** Novel liquid bio-composites were successfully prepared by blending the *N*-methyl diethanolamine (N-MDEA) modified poly (butylene succinate) (N-PBS) and carboxy-methylated cellulose (CMC) or hydroxyl-ethyl cellulose (HEC) in solution. In order to reveal the interaction mechanism between N-PBS and cellulose derivatives, the mixing energy and interaction parameter of (N-PBS)-CMC and (N-PBS)-HEC were calculated using molecular dynamics simulation. In addition, the interaction mechanism of composites was explained using Fourier transform infrared spectroscopy (FTIR), X-ray photoelectron spectroscopy (XPS), and scanning electron microscopy (SEM). The molecular dynamics simulation results indicated that the hydrogen bonding, physical absorption, and electrostatic interaction produced between –OH, –OCO–, –COOH, and –N–$CH_2$– functional groups. The (N-PBS)-HEC composite displayed more stable system than that of (N-PBS)-CMC composite. The results were explained using absorption peak of functional groups in FTIR and the binding energy distribution change of C1s, O1s, and N1s elements in XPS and smooth surface between N-PBS and HEC.

**Keywords** N-PBS · Cellulose derivatives · Liquid composite · Dynamics simulation · Interaction

✉ Min Zhang
yanjiushi206@163.com

Xiao-Ling Xu
xxl101010@126.com

[1] Key Laboratory of Auxiliary Chemistry and Technology for Chemical Industry, Ministry of Education, Shaanxi University of Science and Technology, Xi'an 710021, China

[2] Key Laboratory of Agro-Environment and Climate Change, Ministry of Agriculture, Institute of Environment and Sustainable Development in Agriculture, Chinese Academy of Agricultural Sciences, Beijing 100081, China

[3] Key Laboratory of Dryland Farming and Water-Saving Agriculture, Ministry of Agriculture, Beijing 100081, China

## Introduction

Recently, biodegradable polymer films, instead of petroleum-based plastic films, have gained much interest as natural resource limitation and environmental problems are concerned [1–3]. Thus, the relationship between structure and properties of biodegradable composites has been intensively studied [4, 5]. In recent years, biodegradable aliphatic polyester and natural polymer fiber composite materials have become one of the most effective composites to ease environmental stress for the good performance, low cost, and good biocompatibility [6]. Among those materials, poly (butylene succinate) (PBS) is considered an outstanding biodegradable polyester due to its good film-forming property and good thermodynamic properties compared to other polyesters [7–9]. It is widely used in food packages, agriculture film, biomedicines, and other fields [10–13]. However, the industrialization of PBS has not been widening due to the high price. One of the effective methods to reduce the price is to make bio-composites. Bio-composites are an emerging class of composites formed by the combination of natural polymer and biodegradable polymers [14, 15]. Cellulose derivatives are modified using cellulose which is abundant, renewable, and inexpensive [16]. However, water-soluble carboxymethyl cellulose (CMC), and hydroxyethyl cellulose (HEC) have received much interest due to their non-toxicity, good biocompatibility, high viscosity, transparency, and good film forming ability [17, 18]. A few

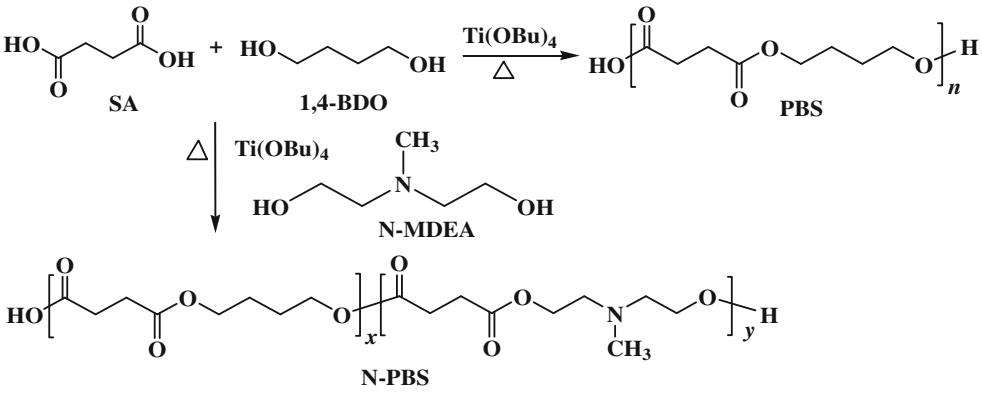


**Fig. 1** Synthesis route of PBS and N-PBS copolymer

reports have been published on the production/preparation of bio-composites by adding modified cellulose. Rhim et al. prepared sodium carboxymethyl cellulose/cotton linter cellulose nano-fibril (CMC/CNF) composite films with good mechanical properties due to the high compatibility between CNF and CMC [19]. Azzaoui et al. manufacated hydroxyapatite/hydroxyethyl (HAp/HECA) inorganic–organic composite films which showed good thermal stability and miscibility due to the strong interaction between HAp and HECA [20]. It was also illustrated that the interaction between composites has a direct impact on the compatibility and the improvement of performance.

In the past few years, interface problem creates huge research scope, which is determined by the interface interaction between the molecules. Recently, certain progress has been achieved through gaining information about interaction mechanism between composite materials using molecular dynamics simulation [21–23]. It indicated that the macro performance was closely related with microstructures. It replaces the traditional testing methods which provide microscopic theory supporting for the macroscopic phenomena. In our previous work, it was found out that the interaction existed between functional groups of composites. In addition, it was also shown using YASARA and Material Studio (MS) simulations that the helixes structure of PBS changed into a linear random chain structure by introducing a third component [24, 25]. In addition, strong interactions are formed between modified PBS copolymer and CMC. However, complicated interaction mechanisms between the bio-composites are still not fully known.

In this paper, YASARA and MS simulation combined with experiments were used to compare the interfacial interaction of bio-composites consisting of biodegradable copolymer N-PBS with CMC and HEC, respectively. The copolymer N-PBS was synthesized by introducing *N*-methyl diethanol amine (N-MDEA) to the main chain of PBS. The interaction parameters and binding energy were determined to elucidate the interaction between composite films.

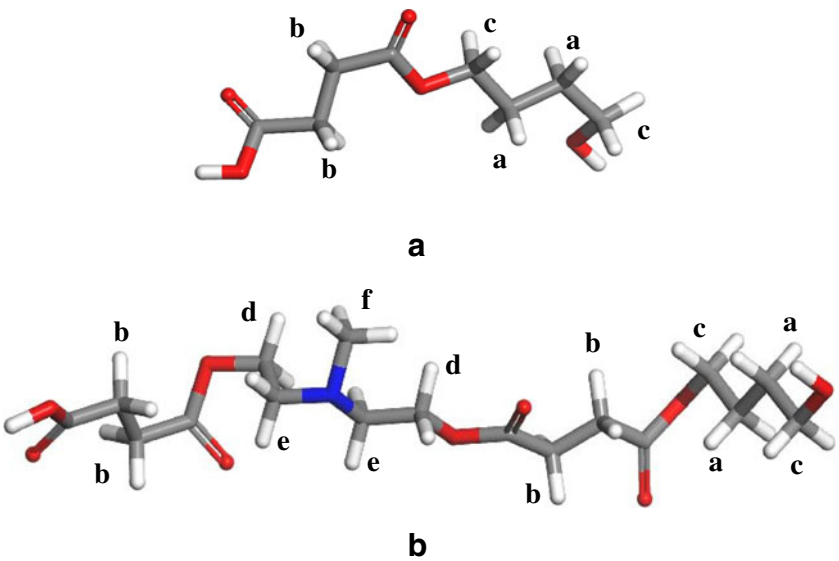


**Fig. 2** Structure unit of **a** PBS and **b** N-PBS copolymer. H—*white*, C—*gray*, O—*red*, N—*blue*

**Table 1** $^1$H NMR data of PBS and N-PBS copolymer

| Polymer | $\delta \times 10^{-6}$ | Serial number | Ownership | Structural units |
|---|---|---|---|---|
| TMS | 0 | – | $-CH_3$ | $(CH_3)_4Si$ |
| PBS | 1.68 | a | $-CH_2-$ | 1,4-BDO |
| | 2.63 | b | $-CH_2-C=O$ | SA |
| | 4.13 | c | $-CH_2-O-$ | 1,4-BDO |
| N-PBS (20 %) | 1.68 | a | $-CH_2-$ | 1,4-BDO |
| | 2.63 | b | $-CH_2-C=O$ | SA |
| | 4.13 | c | $-CH_2-O-$ | 1,4–BDO |
| | 4.18 | d | $-CH_2-O-$ | MDEA |
| | 2.71 | e | $-N-CH_2-$ | MDEA |
| | 2.35 | f | $-N-CH_3$ | MDEA |
| Solvent | 7.26 | – | –C–D– | $CDCl_3$ |

## Experiments

### Materials

Succinic acid (SA, AR) and polyvinyl alcohol (PVA, As-Received) were supplied by Sinopharm Chemical Reagent Company Limited. 1,4-Butanediol, (1,4-BDO, AR), carboxymethyl cellulose (CMC, 800 mPa·s) and glycerol (AR) were provided by Fuchen Chemical Reagents Factory (Tianjing China). *N*-methyldiethanolamine (N-MDEA, Commercially Pure) was supplied by Recovery Fine Chemical Company Limited (Tianjing China). Hydroxyethyl cellulose (HEC, LR) was obtained from Kelon Chemical Reagent Factory (Chengdu, China). Stannous chloride ($SnCl_2$, AR) was supplied by Guanghua chemical plants Company Limited (Guangdong, China). Phosphate ester anionic surfactant (PLYSURF A210G, AR) was given by the First Industrial Pharmaceutical Company Limited (Japan). Industrial grade silane coupling agent (KH550) was supplied by RON Silicon Material Company Limited (Nanjing, China).

### The synthesis of PBS and N-PBS copolymers

The PBS and N-PBS copolymers were synthesized using melt poly-condensation method where a mole ratio of 1:1.1 for SA and 1, 4-BDO [26]. In order to produce N-PBS, 5, 10, 15, 20, 25, 25, 30, 35, and 40 % of N-MDEA was used, respectively. The synthetic route is shown in Fig. 1. Molecular weight of polymers was about $1.0 \times 10^4$, and the distribution coefficient was from 1.83 to 2.31. Structural characteristics of PBS and N-PBS are displayed in Fig. 2. In addition, $^1$H NMR data were shown in Table 1. Strong proton absorption peaks in $\delta$2.35, $\delta$2.71, and $\delta$4.18 are characteristic peaks of N-MDEA. This indicates that expected products were achieved. The products films with thickness of 2 mm were formed from the teflon plate using hot press molding. The contact angle of PBS-based copolymer decreased dramatically with increasing N-MDEA content (Fig. 3), which showed good hydrophilicity for N-PBS.

### The preparation of (N-PBS)-CMC and (N-PBS)-HEC composite films

The liquid composites containing N-PBS and cellulose derivatives (CMC and HEC) solutions were prepared by solution method. The chloroform solution of polymer with 10 mass % N-PBS was emulsified by 0.05 % polyether phosphate ester surfactant (PLYSURF) solution for 2 h. Ten mass % CMC and HEC solutions were used as ligand and mixed with polymer emulsions at 50 °C for 2 h. The additives, such as plasticizer glycerol and filmogen PVA, and coupling agent KH550 with water were added into the mixing emulsions at 50 °C for 1 h. The corresponding biomass liquid composite films were molded after putting 20 g emulsions into PTFE plate and dried at room temperature.

### Performance testing and characterization

Nuclear Magnetic Resonance Spectrometer (ADVANCE III $^1$H NMR, Bruker Company, Germany) was employed to analysis the structure of polymers at 400 MHz and $CDCl_3$ as solvent. Gel permeation chromatograph (P230 GPC, analysis instrument Company Limited, Dalian, China) was employed to determine the molecular weight of polymer where $CHCl_3$ was used as solvent.

YASARA was used to simulate the interaction process under the condition of a water phase system at 323 K. Materials Studio V 7.0 (MS, Accelrys Company, America) was used to investigate the mixing energy and interaction parameter of

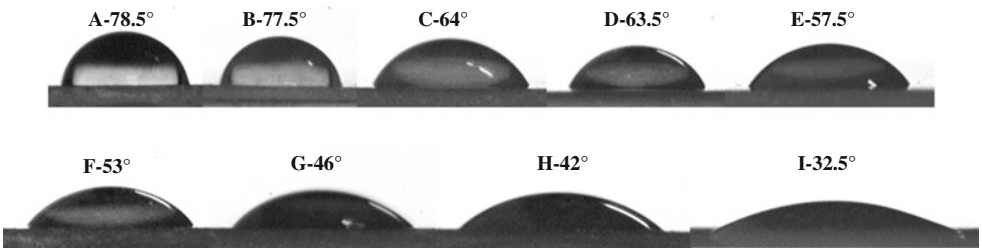


**Fig. 3** Contact angle of (*A*) PBS and (*B*~*I*) N-PBS (5 ~ 40 %) copolymers

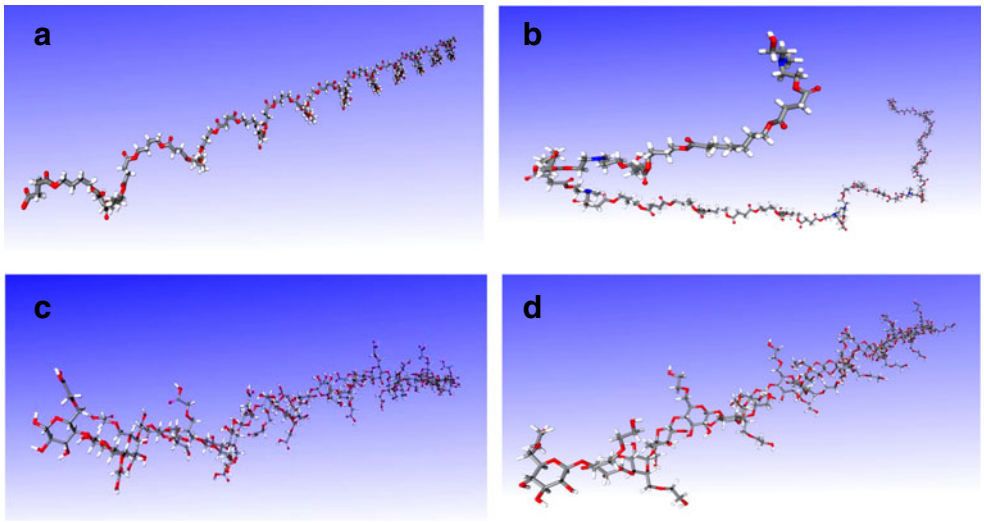


**Fig. 4** The structure of PBS (**a**), N-PBS (**b**), CMC (**c**), and HEC (**d**). H—*white*, C—*gray*, O—*red*, N—*blue*

(H-white, C-gray, O-red, N-blue)

composites. The force field was compass; the charge was QEq, atom-based van der Waals (VDW) at the isothermal-isobaric ensemble (NPT) with 298 K and 1 bar.

Fourier transform infrared spectrometer (VECTOR-22 FTIR, Bruker Company, Germany) was used to analyze the structures of composites at room temperature operating at the range of 4000 ~ 600 $cm^{-1}$.

X-ray photoelectronic spectroscopy (Vario EL III XPS, Elemental Analyzing system GmbH, Germany) was used to analyze the distribution of elements on the surface of composites. XPS analyses were carried out using a monochromatic Al K$\alpha$ ($h\nu$ = 1486.7 eV) X-ray source, at 150 W (10 mA, 15 kV). Survey spectra were acquired for binding energies in the range 0–1200 eV. C1s, O1s, and N1s region spectra were acquired after fitting the peak processing obtained higher spectral resolution. Spectra were analyzed using the Casa XPS software (version 2.3.16) and have been corrected to the main line of the carbon C1s, O1s, and N1s spectral component.

Scanning electron microscopy (S-4800 SEM, Rigaku Company Limited, Japan) was used to observe the surface topography of the composite films which operated at 10 kV with spot size of 10 nm.

## Results and discussion

### Dynamics simulation of composite materials in the liquid phase system

The structures of PBS, N-PBS, CMC, and HEC with 25 repeated units were displayed in Fig. 4. PBS revealed a regular helix chain showing the conformation regularity (Fig. 4a) [27]. However, N-PBS displayed random torsion structure which could increase the flexibility of chain (Fig. 4b). The introduction of N-MDEA changes the regularity of PBS chain and could effectively improve the flexibility. The random structure of N-PBS displayed good hydrophilia which explains the contact angle results. The structure of CMC (Fig. 4c) and HEC (Fig. 4d) shows a line torsion structure with the main chain of hexatomic

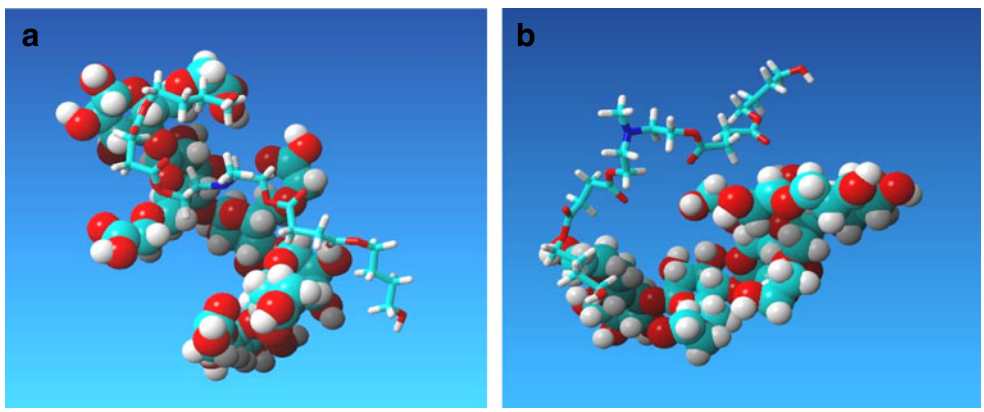


**Fig. 5** Molecular dynamics simulation images of **a** (N-PBS)-CMC and **b** (N-PBS)-HEC composites in aqueous solution

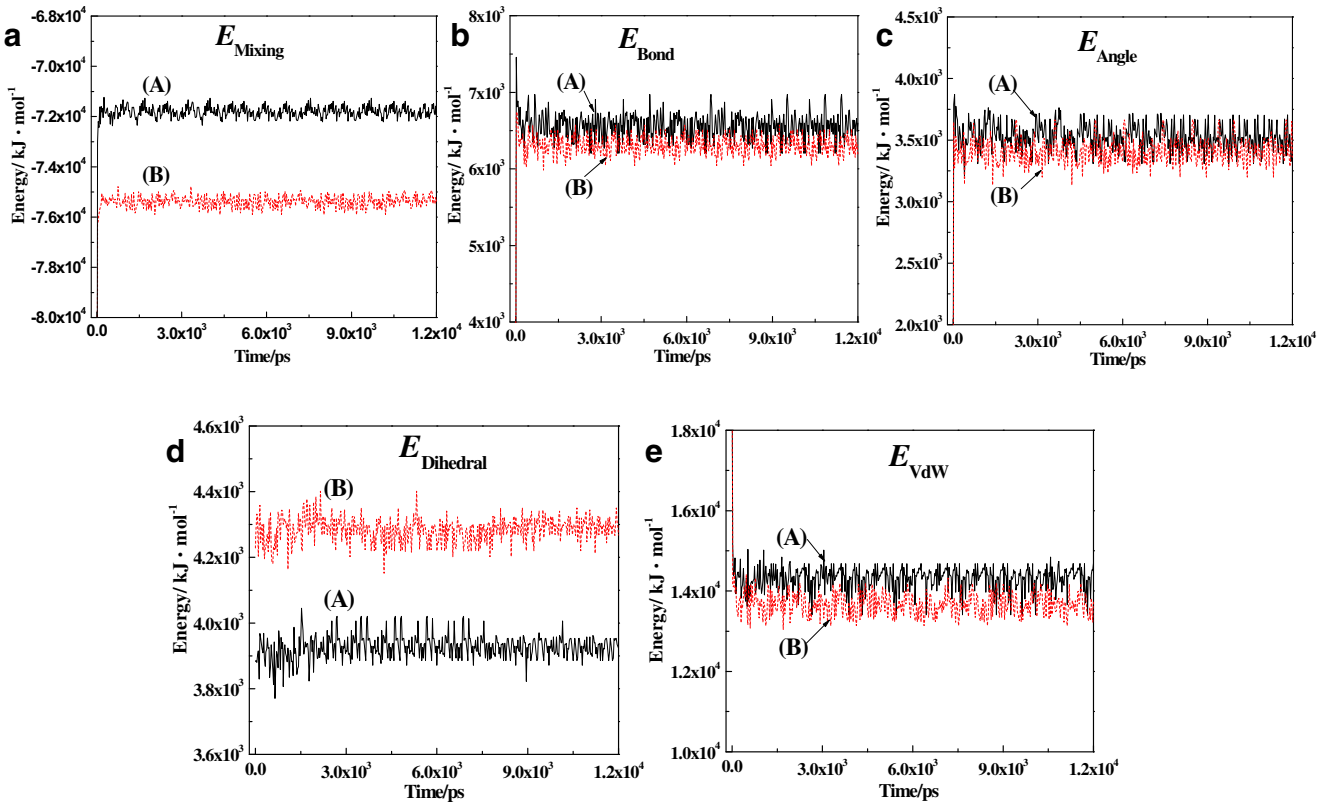


[(a) $E_{Mixing}$ (b) $E_{Bond}$ (c) $E_{Angle}$ (d) $E_{Dihedral}$ (e) $E_{VdW}$]

**Fig. 6** Interaction energy of (*A*) (N-PBS)-CMC and (*B*) (N-PBS)-HEC composites. **a** $E_{Mixing}$, **b** $E_{Bond}$, **c** $E_{Angle}$, **d** $E_{Dihedral}$, and **e** $E_{VdW}$

rings. Further, functional groups dispersed outside the main chain of CMC and HEC provided an interaction platform with N-PBS.

Dynamic simulation system was designed in a water solvent to determine the interaction energy of (N-PBS)-CMC and (N-PBS)-HEC composites (Fig. 5). The size of the solvent box was 3.85 nm × 3.85 nm × 3.85 nm with periodic boundary [24]. Then, N-PBS with stick model was mixed with CMC and HEC with a spherical model at 323 K, respectively. It was found that (N-PBS)-HEC has lower kinetic mixing energy of $-7.2 \times 10^4$ kJ·mol$^{-1}$ under the condition of water solvent (Fig. 6a). The energy tended to be stable for less than 200 ps indicating good miscibility and stability of the composites. The angle, bond and van der Waals energy were almost the same for (N-PBS)-CMC and (N-PBS)-HEC composites. Figure 6b, c, e displayed that hydrogen bonding, adsorption [28], and van der Waals force occurred between N-PBS and cellulose derivatives, respectively. The dihedral energy of (N-PBS)-HEC was higher than that of (N-PBS)-CMC shown in Fig. 6d due to the higher dihedral energy of HEC than that of CMC. The average energy of CMC, HEC, and their composites are shown in Tables 2 and 3. It illustrates that the introduction of N-PBS can influence the energy of the blend system. All the energies decrease when the N-PBS is added in the blend system. Interestingly, the impact values of N-PBS are a little greater on the (N-PBS)-HEC than that of (N-PBS)-CMC except for mixing energy. It indicates that N-PBS involves in the interaction between two kinds of

**Table 2** Interaction energy of CMC, HEC, and (N-PBS)-CMC, (N-PBS)-HEC composites

| Energy | CMC | (N-PBS)-CMC | Impact value of N-PBS | HEC | (N-PBS)-HEC | Impact value of N-PBS |
|---|---|---|---|---|---|---|
| $E_{Mixing}$/×10$^4$ kJ·mol$^{-1}$ | −7.52 | −7.18 | −0.34 | −7.97 | −7.54 | −0.43 |
| $E_{Bond}$/×10$^3$ kJ·mol$^{-1}$ | 7.12 | 6.55 | 0.57 | 7.08 | 6.30 | 0.78 |
| $E_{Angle}$/×10$^3$ kJ·mol$^{-1}$ | 3.92 | 3.53 | 0.39 | 3.87 | 3.41 | 0.46 |
| $E_{Dihedral}$/×10$^3$ kJ·mol$^{-1}$ | 6.34 | 3.93 | 2.41 | 7.12 | 4.28 | 2.84 |
| $E_{VdW}$/×10$^4$ kJ·mol$^{-1}$ | 1.52 | 1.43 | 0.09 | 1.51 | 1.36 | 0.15 |

**Table 3** Interaction energy and interaction parameter of composites

| Composites | $E_{mixing}$/ kJ·mol$^{-1}$ | $\chi$ | $E_{potential}$/×10$^4$ kJ·mol$^{-1}$ | $E_{nonbond}$/×10$^4$ kJ·mol$^{-1}$ | CED/×10$^8$ J·m$^{-3}$ | $\delta$ / (J·m$^{-3}$)$^{0.5}$ |
|---|---|---|---|---|---|---|
| (N-PBS)-CMC | 182.62 | 74.26 | 3.83 | 2.31 | 3.79 | 19.48 |
| (N-PBS)-HEC | −53.22 | −20.49 | 0.44 | 0.26 | 3.89 | 19.68 |

composites. The blend (N-PBS)-HEC may have stronger hydrogen bonding, adsorption, and van der Waals force.

The blends module in MS was used to predict and calculate the miscibility of the N-PBS and cellulose derivative composites [29, 30]. Figure 7 shows the amorphous unit cells of (N-PBS)-CMC and (N-PBS)-HEC composites. Tables 2 and 3 show binding energy as mixing energy ($E_{mixing}$), potential energy ($E_{potential}$), and non-bond energy ($E_{nonbond}$) and interaction parameters, such as Flory-Huggins parameter ($\chi$), cohesive energy density (CED), and solubility parameter ($\delta$) after simulation for 500 ps. The monomers of N-PBS, CMC, and HEC were introduced into polymer builder modules with optimized structure. Then, N-PBS, CMC, and HEC polymers with 25 polymerization degrees (DP25) were built using build polymer module and energy minimized using discover dynamic module. The mixing systems for (N-PBS)-CMC and (N-PBS)-HEC are constructed using an amorphous cell module with one molecular chain for each component and made dynamic simulation in the module of MS Discover. The sampling period of simulation was carried out at NPT ensemble from 0 to 500 ps. It is evident that (N-PBS)-HEC composites displayed lower $E_{mixing}$ (−53.22 kJ·mol$^{-1}$), $E_{potential}$ ($0.44 \times 10^4$ kJ·mol$^{-1}$), and $E_{nonbond}$ ($0.26 \times 10^4$ kJ·mol$^{-1}$) than (N-PBS)-CMC composites. This implies a more stable mixing system for (N-PBS)-HEC composites. In addition, the lower parameter $\chi$ (−20.49) of (N-PBS)-HEC composite indicates a better compatibility and stability.

CED and $\delta$ are used to evaluate the intermolecular interaction, which mainly reflects the interaction between the functional groups [31]. It is well-established that greater polarity of the groups in molecules represents greater intermolecular interactions. However, higher CED and $\delta$ parameters indicate greater polarity of the molecules [32]. It is obvious that (N-PBS)-HEC composites own relatively high value of CED and $\delta$ parameter indicating a strong interaction existed between polar groups in the molecular chain-formed hydrogen bond, electrostatic adhesion, and van der Waals interaction.

Radial distribution function g(r) is used to characterize microstructure of materials and reveals the essence of the interaction [33]. The functions estimate the type of interaction force and the strength of the force in terms of peak position and the peak height, respectively. Figure 8 shows g(r) of the atomic pairs of (N-PBS)-CMC and (N-PBS)-HEC composites. The peak distributions value, r of less than 0.5 nm for both composites, reveals the existence of intermolecular and intra-molecular interaction between composites [34]. The values from 0 to 0.13 nm indicate covalent forces between

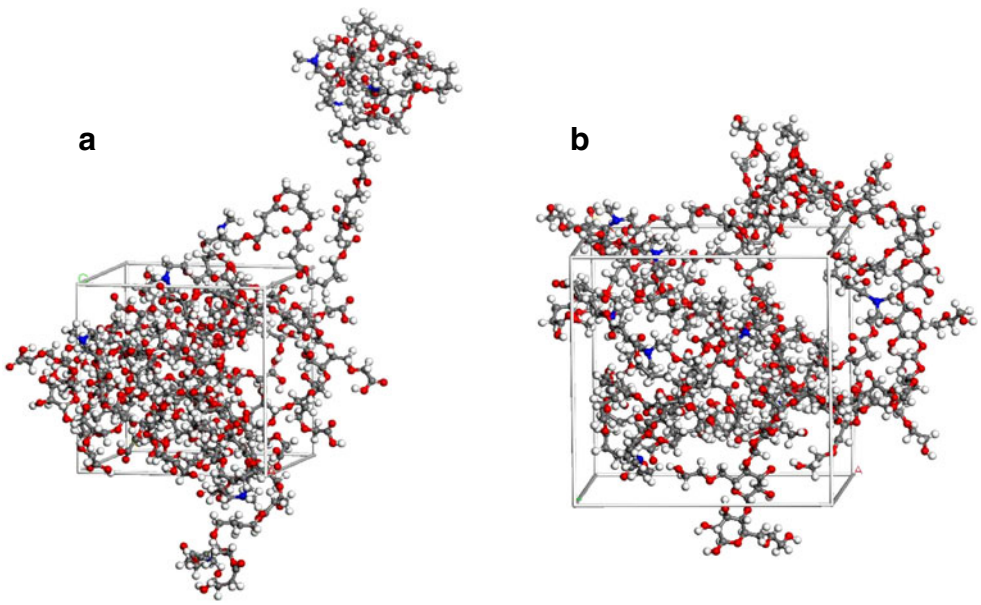


**Fig. 7** Micrographs of the amorphous unit cells of (**a**) (N-PBS)-CMC and (**b**) (N-PBS)-HEC. H—*white*, C—*gray*, O—*red*, N—*blue* (H-white, C-gray, O-red, N-blue)

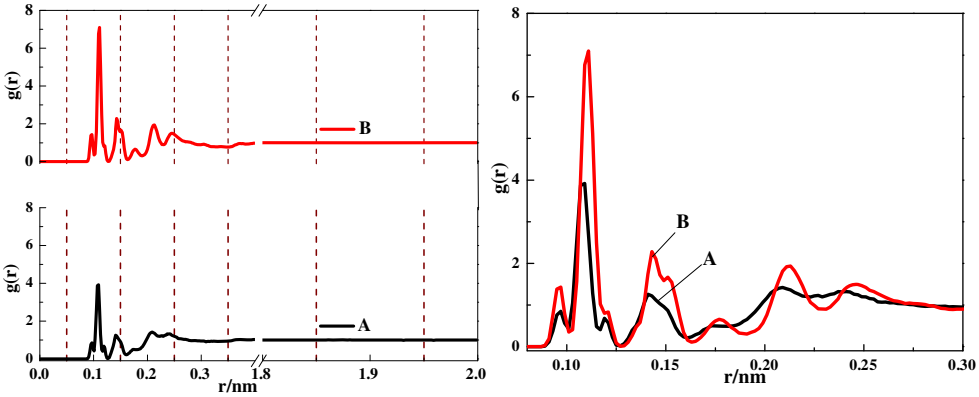


**Fig. 8** Radial distribution functions of (*A*) (N-PBS)-CMC and (*B*) (N-PBS)-HEC composites at 298 K

C–C, C–O, C–H, and C–N bonds in polymers. On the other hand, hydrogen-bonding and electrostatic interactions are assigned to 0.13 ~ 0.3 nm attributed to the O–H and N–H bonds. The VdW force is too weak to display when $r > 0.3$ nm indicating that the main interactions in N-PBS and CMC (HEC) composites are hydrogen-bonding and electrostatic interactions. It is worth mentioning that g(r) of (N-PBS)-HEC composite is higher than that of (N-PBS)-CMC composite. This means a stronger interaction existed between N-PBS and HEC.

Figure 9 shows the mean-squared displacements (MSD) indicating the dynamics of composites in the last 300-ps trajectory. In statistical mechanics, MSD is the most common measure of the spatial extent of random motion which indicates the speed of diffusion [35, 36]. Then, MSD curves and the regular residual are used to illustrate the mobility of composites. The fitted MSD in Fig. 9 displays linear distribution for both of composites. The correlation coefficients ($R^2$) of (N-PBS)-CMC and (N-PBS)-HEC are found to be 0.9400 and 0.9697, respectively. In contrast, the blend system of (N-PBS)-HEC remained relatively stable from 50 to 200 ps. The residual of (N-PBS)-HEC is about 0.1 floating up and down, and (N-PBS)-CMC is about 0.15 floating up and down. This indicates that the mobility of (N-PBS)-CMC was bigger than that of (N-PBS)-HEC composite. The aforementioned results are indicatives of strong interaction between N-PBS and HEC composite.

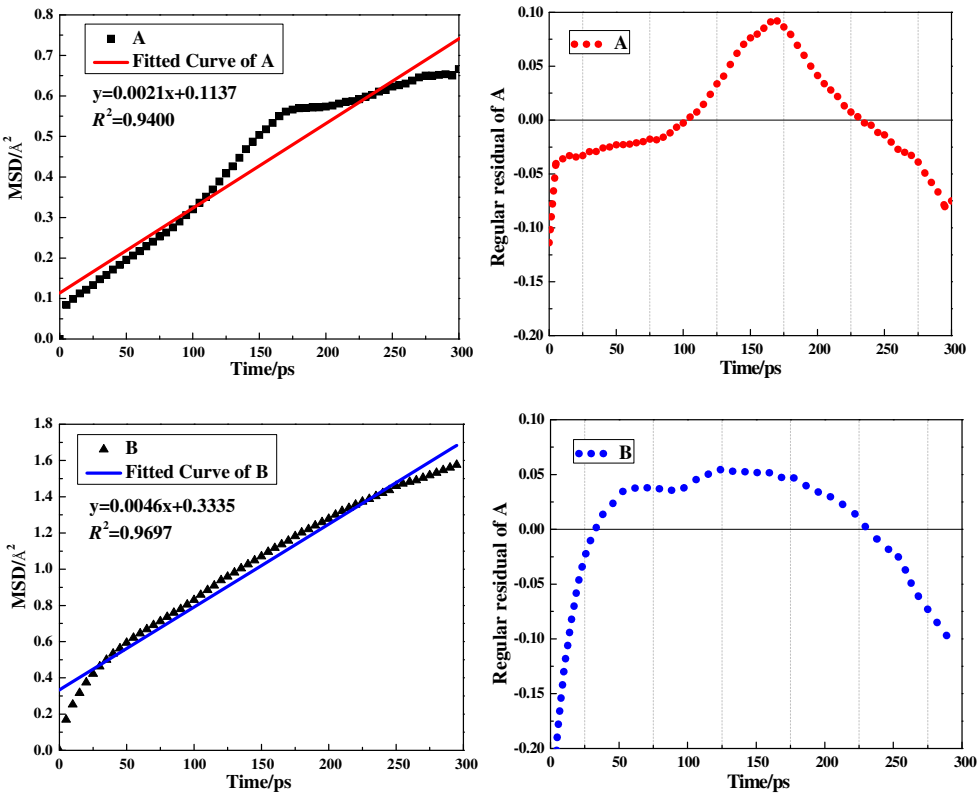


**Fig. 9** Mean-squared displacements and residual of (*A*) (N-PBS)-CMC and (*B*) (N-PBS)-HEC composites

### The FTIR characterization of the composite films

FTIR spectra of (N-PBS)-CMC and (N-PBS)-HEC composite films are shown in Fig. 10. It is evident that the spectrum shape of films is roughly similar with certain deviation in characteristic peak. A wide hydroxyl (−OH) vibration absorption band appeared in 3331 ~ 3342 $cm^{-1}$ for both composite films. There is a difference in absorption displacement and strength between (N-PBS)-HEC and (N-PBS)-CMC composite. The absorption displacement showed a little shift, and the absorption strength decreased which manifests stronger interaction existed between N-PBS and HEC composites. The peaks at 2950 and 2872 $cm^{-1}$ are attributed to the $–CH_2–$ asymmetrical stretching vibration and the symmetrical stretching vibration, respectively. The stretching vibration absorption peak at 1721 $cm^{-1}$ corresponds to –C=O. In addition, the stretching vibration of –COO– reflects at 1329 and 1154 $cm^{-1}$. However, the peak at 1046 $cm^{-1}$ is for the symmetric stretching vibration of O–C. Due to the influence of hydrogen bond interaction, the absorption strength increased for (N-PBS)-HEC composites. The peak at 1420 $cm^{-1}$ arose from the C–N–C asymmetrical stretching vibration, and the peak at 1656 $cm^{-1}$ stood for the asymmetrical stretching vibration of N–C. The slight change in absorption position and the absorption strength might be attributed to the effects of hydrogen bond and adsorption between –OH, −COO–, and C–N functional groups of composites.

### The XPS analysis of the composite films

X-ray photoelectron spectroscopy (XPS) is the well-suited technique to examine the possible interactions between polymer-cellulose interphase [37]. XPS results showed that the two membrane surfaces predominantly contain carbon, oxygen, and nitrogen (90 %). Figure 11 shows the low-resolution XPS spectra of (N-PBS)-CMC and (N-PBS)-HEC composites. The atomic contents of different elements in (N-PBS)-CMC were 26.02 % (O1s), 63.07 % (C1s), and 2.37 % (N1s). This was different from (N-PBS)-HEC containing 24.57 % (O1s), 67.43 % (C1s), and 1.16 % (N1s). The (N-PBS)-HEC composite showed higher C content and lower O and N content at the surface as a result of the strong interaction. It is worth mentioning that the carbon spectrum showed six different chemical states. However, oxygen and nitrogen had three and two different chemical states, respectively. The binding energy ($E_{binding}$) of the three elements displayed large difference for the two kinds of composites. $E_{binding}$ for O1s and N1s of (N-PBS)-HEC is found to be much higher than that of (N-PBS)-CMC. It indicates that inter- and intra-chain hydrogen bonding, physical adsorption, and VdW interaction display higher impact on the binding energy of (N-PBS)-HEC than that of (N-PBS)-CMC composite.

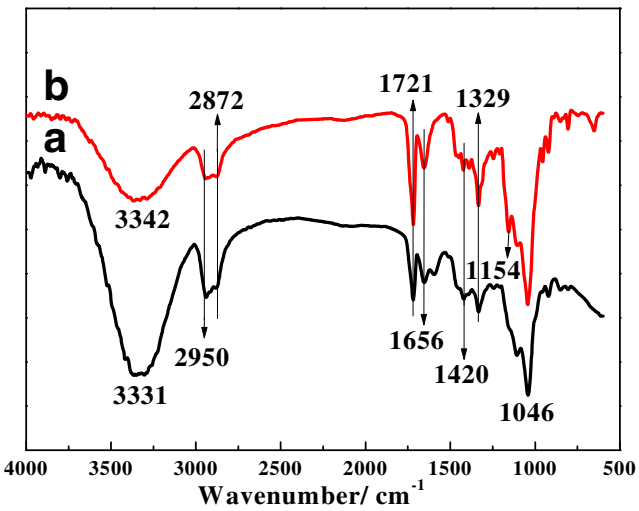


**Fig. 10** FTIR of (N-PBS)-CMC (**a**) and (N-PBS)-HEC (**b**) composites

Composition of (N-PBS)-CMC composite was determined based on the intensity of the C1s, O1s, and N1s peaks at 283, 529, and 397 eV, respectively [38]. Similar results have been observed for the (N-PBS)-HEC composite film. The binding energies of O1s, C1s, and N1s are given in Table 4. The C1s spectrum of (N-PBS)-CMC showed six carbon environments corresponding to C–C and C–H (284.60 eV), C–O (286.30 eV), C=O (287.92 eV), O–C=O (292.86 eV), and $C–N(CH_3)$ (285.31 eV) groups. The intensity of –O–C=O chemical bonding in (N-PBS)-HEC composite was too low to detect/branch off from the C1s spectrum. This indicates the occurrence of interaction and overlapping between the ester group and other groups. The intensity of three chemical states of O1s was relatively lower in (N-PBS)-HEC, and the $E_{Binging}$ was moved 2 eV in the direction of large energy that might be used as an indicator of the presence of interaction between the oxygen containing groups. A similar peak changing trend with binding energy shift was also observed for the N1s spectrum, suggesting that interaction existed between amide functional groups.

### The SEM of (N-PBS)-CMC and (N-PBS)-HEC composite films

Figure 12 shows the surface and the interface morphology of the two kind of composite films. The (N-PBS)-CMC surface shows a relatively rough surface with obvious stratification (Fig. 12a). In contrast, the (N-PBS)-HEC surface was smooth indicating better compatibility between N-PBS and HEC composite (Fig. 12b). It should be mentioned that hydrophilic N-PBS adhered and interlocked into the colloid cellulose, and hydrogen bonding made polyester absorbent on the interface of cellulose. The colloid structure of CMC or HEC interlocks

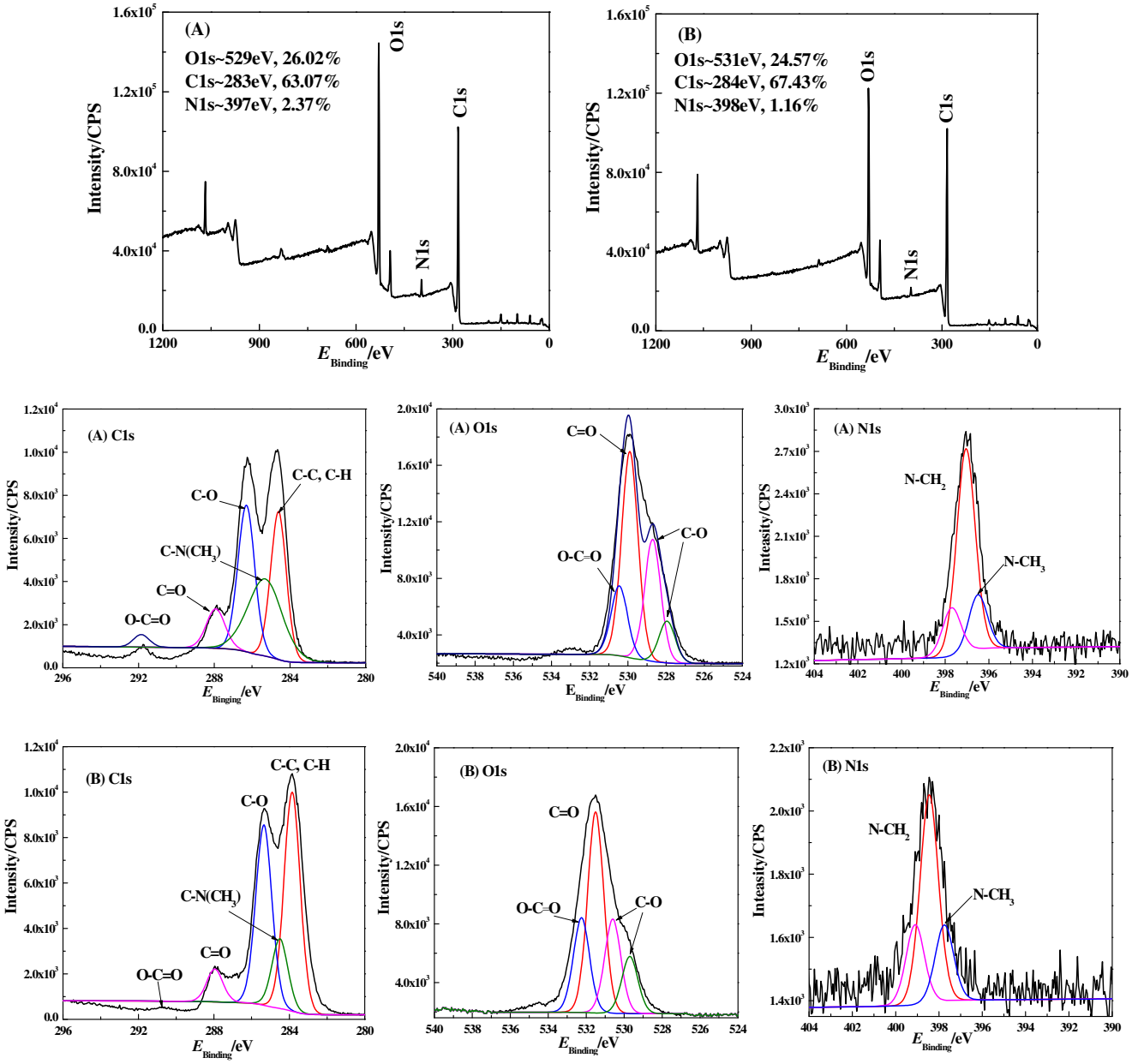


**Fig. 11** XPS spectra of (*A*) (N-PBS)-CMC and (*B*) (N-PBS)-HEC composites and the binding energy distribution of C1s, O1s, and N1s

with the N-PBS copolymer, which increases the compatibility. Functional groups in HEC were much easier to interact with N-PBS, and the interface interaction was stronger, which agrees with the results predicted using simulation.

## Conclusions

The N-MDEA modified PBS displayed good hydrophilia and compatibility of cellulose derivatives. Dynamics simulation

**Table 4** Binding energy for high resolution XPS spectra of C1s, O1s, and N1s elements in composites

| Bond type Composites | C(1 s)Binding energy (eV) | | | | | O(1 s)Binding energy (eV) | | | N(1 s)Binding energy (eV) | |
|---|---|---|---|---|---|---|---|---|---|---|
| | C–C, C–H | C–O | C=O | O–C=O | C–N($CH_3$) | C–O | C=O | O–C=O | N–$CH_3$ | N–$CH_2$ |
| (N-PBS)-CMC | 284.60 | 286.30 | 287.92 | 291.86 | 285.31 | 527.93, 528.75 | 530.27 | 533.17 | 396.48 | 397.04, 397.68 |
| (N-PBS)-HEC | 283.85 | 285.35 | 287.95 | 290.67 | 284.50, 283.25 | 529.72, 530.06 | 531.48 | 532.26 | 397.76 | 398.43, 399.13 |

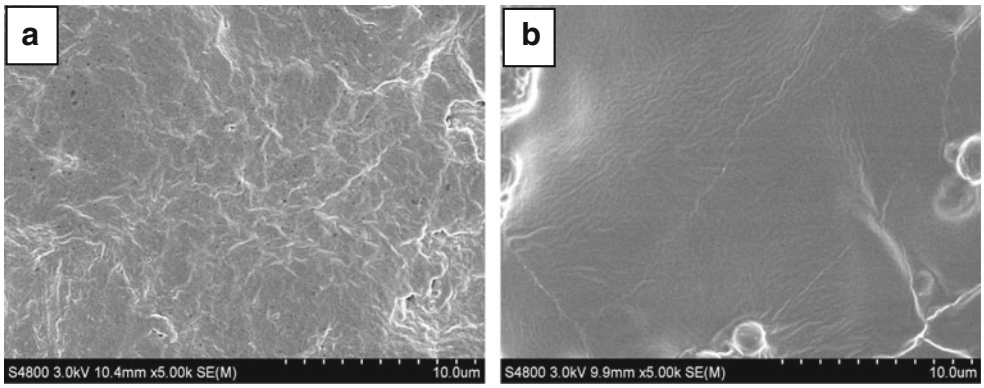


**Fig. 12** SEM images of surface of liquid composite films. **a** (N-PBS)-CMC, **b** (N-PBS)-HEC

theoretically calculated the binding energy and interaction parameters of composites which indicated that non-covalent interaction, such as hydrogen bonding, physical absorption, electrostatic repulsion, and VdW force, existed in N-PBS and cellulose derivatives. It was explained using the functional groups peak obtained from FTIR and the binding energy changed. The interactions in –OH, OCO–, $-N-CH_2-$, and –COOH functional groups were favorable improving the compatibility of composites. It was found that (N-PBS)-HEC displayed more stable blend system and better compatibility due to the lower binding energy, $\chi$ and the mobility, the larger CED, $\delta$ and $R^2$, and smooth surface. Furthermore, the interaction mechanism and the relationship between structure and properties of biodegradable composites remain to be further researched.

**Acknowledgments** This review was made possible by the financial support of the National High-Tech R & D Program (863 Program) for the 12th Five-Year Plan (2011AA100503). We would also like to thank Prof. Ji-Qing Song and Wen-Qing He for their assistance.

**Compliance with ethical standards**

**Conflict of interest** The authors declare that they have no competing interests.

## References

1. Ammala A, Bateman S, Dean K, Petinakis E et al (2010) An overview of degradable and biodegradable polyolefins. Prog Polym Sci 36(8):1015–1049
2. Tania FF, Eliane T, Freire CSR et al (2011) Preparation and characterization of novel biodegradable composites based on acylated cellulose fibers and poly(ethylene sebacate). Compos Sci Technol 71(16):1908–1913
3. Xiong Z, Ma SQ, Fan LB, Tang ZB, Zhang RY et al (2014) Surface hydrophobic modification of starch with bio-based epoxy resins to fabricate high-performance polylactide composite materials. Compos Sci Technol 94:16–22
4. Huang GQ, Cheng LY, Xiao JX, Han XN (2015) Preparation and characterization of *O*-carboxymethyl chitosan–sodium alginate polyelectrolyte complexes. Colloid Polym Sci 293(2):401–407
5. Awal A, Rana M, Sain M (2015) Thermorheological and mechanical properties of cellulose reinforced PLA bio-composites. Mech Mater 80:87–95
6. Ashok B, Obi Reddy K, Madhukar K, Cai J, Zhang L, Varada Rajulu A (2015) Properties of cellulose/thespesia lampas short fibers bio-composite films. Carbohydr Polym 127:110–115
7. Ding ML, Zhang M, Yang JM (2012) Study on the enzymatic degradation of aliphatic polyester-PBS and its copolymers. J App Polym Sci 124:2902–2907
8. Elisabete F, Nadia B, Laura S, Annamaria C (2015) Biocomposites based on poly(butylene succinate) and curaua: mechanical and morphological properties. Polym Test 45:168–173
9. Zhou M, Li YH, He C, Jin TY, Wang K, Fu Q (2014) Interfacial crystallization enhanced interfacial interaction of poly (butylene succinate)/ramie fiber biocomposites using dopamine as a modifier. Compos Sci Technol 91:22–29
10. Schettini E, Santagata G, Malinconico M et al (2013) Recycled wastes of tomato and hemp fibres for biodegradable pots: physico-chemical characterization and field performance. Conserv Recycl 70(1):9–19
11. Bajpai PK, Meena D, Vatsa S, Singh I (2013) Tensile behavior of nettle fiber composites exposed to various environments. J Nat Fiber 10(3):244–256
12. Zhang M, Xing YL, Su KY, Ma YQ, Song JQ (2011) Degradation of PBS-based copolymers and impacts on the growth of winter wheat. Agric Sci Technol 12(9):1362–1366
13. Frollini E, Bartolucci N, Sisti L et al (2013) Poly(butylene succinate) reinforced with different lignocellulosic fibers. Ind Crops Prod 45(2):160–169
14. Yu T, Hu CQ, Chen XJ, Li Y (2015) Effect of diisocyanates as compatibilizer on the properties of ramie/poly(lactic acid) (PLA) composites. Compos A: Appl Sci Manuf 76:20–27
15. Tapasi M, Michael C, Nhol K et al (2014) Dispersion study of nanofibrillated cellulose based poly (butylene adipate-*co*-terephthalate) composites. Carbohydr Polym 102(2):537–542
16. József KK, Haroon M, Alessandro P (2015) Recent advances in fiber/matrix interphase engineering for polymer composites. Prog Mater Sci 73:1–43
17. Wang JJ, Feng M, Zhan HB (2014) Preparation, characterization, and nonlinear optical properties of graphene oxide-carboxymethyl cellulose composite films. Optics Laser Technol 57:84–89
18. Kang HL, Liu RG, Huang Y (2015) Graft modification of cellulose: methods, properties and applications. Polym 70:1–16
19. Oun AA, Rhim JW (2015) Preparation and characterization of sodium carboxymethyl cellulose/cotton linter cellulose nanofibril composite films. Carbohydr Polym 127:101–109

20. Azzaoui K, Mejdoubi E, Lamhamdi A, Zaoui S et al (2015) Structure and properties of hydroxyapatite/ hydroxyethyl cellulose acetate composite films. Carbohydr Polym 115:170–176
21. Poghosyan AH, Arsenyan LH, Antonyan LA et al (2015) Molecular dynamics simulations of branched polyethyleneimine in water-in-heptanol micelles stabilized by zwitterionic surfactants. Colloids Surf A: Physicochem Eng Asp 479:18–24
22. Mehran S, Rouhi S, Salmalian K (2015) Molecular dynamics simulations of the adsorption of polymer chains on graphyne and its family. Physica B 456:41–49
23. Arenaza Inger M, Meaurio E, Coto B, Sarasua JR (2010) Molecular dynamics modelling for the analysis and prediction of miscibility in polylactide/polyvinilphenol blends. Polym 51:4431–4438
24. Zhang M, Xu XL, Song JQ, He WQ (2015) Interfacial interaction mechanism of etherified PBS and CMC liquid composites. Chem J Chin U 36(4):808–814
25. Xu XL, Zhang M, Song JQ, He WQ (2014) Preparation and interaction of modified PHS and CMC liquid composites. Adv Mater Res Vol 1035:204–211
26. Zhang M, Lai SL, Song J, Qiu JH (2008) Copolymerization and modification of biodegradable poly(butylene succinate) by 1, 4-CHDM. Chem J Chin U 29(6):1243–1246
27. Eiji Y, Katsuhiro M, Hiroki I, Yoshio F, Kanji N (2009) Helical polymers: synthesis, structures, and functions. Chem Rev 109 (11):6102–6211
28. Dunnington BD, Schmidt JR (2015) Molecular bonding-based descriptors for surface adsorption and reactivity. J Catal 324:50–58
29. Zhao GZ, Feng YB, Fu YZ et al (2009) Molecular dynamic simulations and mesoscopic dynamic simulations on the compatibility of HTPB/plasticizer blends. Acta Chim Sin 67 (19):2233–2238
30. Yang J, Zhao JJ, Han CR, Duan JF (2014) Keys to enhancing mechanical properties of silica nanoparticle composites hydrogels: the role of network structure and interfacial interactions. Compos Sci Technol 95:1–7
31. Yang JQ, Gong XD, Wang GX (2015) Compatibility and mechanical properties of BAMO-AMMO/DIANP composites: A molecular dynamics simulation. Comput Mater Sci 102:1–6
32. Gupta J, Nunes C, Vyas S, Jonnalagadda S (2011) Prediction of solubility parameters and miscibility of pharmaceutical compounds by molecular dynamics simulations. J Phys Chem B 115(9):2014–2023
33. Qi XF, Zhang XH, Li JZ et al (2013) Molecular dynamics simulation of NC/NG blends. Acta Armamentarii 34(1):93–99
34. Fu Y, Liao L, Lan Y et al (2012) Molecular dynamics and mesoscopic dynamics simulations for prediction of miscibility in polypropylene/polyamide-11 blends. J Mol Struct 1012:113–118
35. Alexander GY (1999) Analytic and geometric background of recurrence and non-explosion of the brownian motion on riemannian manifolds. Bull Amer Math Soc 36:135–249
36. Im S, Kim H et al (2016) On the mean square displacement of a random walk on a graph. Eur J Comb 51:227–235
37. Baer DR, Engelhard MH (2010) XPS analysis of nanostructured materials and biological surfaces. J Electron Spectrosc Relat Phenom 178–179:415–432
38. Xu GQ, Wang LH, Liu JL, Wu JZ (2013) FTIR and XPS analysis of the changes in bamboo chemical structure decayed by white-rot and brown-rot fungi. Appl Surf Sci 280:799–805